

Phase conversion dissipation in multi-component compact stars

Mark G. Alford, Sophia Han (韩君), Kai Schwenzer

Physics Department, Washington University, St. Louis, MO 63130, USA

(Dated: 21 Apr 2014)

We propose a mechanism for the damping of density oscillation modes in multi-component compact stars. The mechanism is the periodic conversion between different phases, i.e. the movement of their interface, induced by pressure oscillations in the star. The damping grows nonlinearly with the amplitude of the mode. We study in detail the case of r-modes in a hybrid star with a sharp interface, and we find that this mechanism can saturate the r-mode at a low saturation amplitude and could therefore be the dominant r-mode saturation mechanism in hybrid stars.

PACS numbers: 25.75.Nq, 26.60.-c, 97.60.Jd,

I. INTRODUCTION

The damping of mechanical oscillations of compact stars is a promising signature of the phases of dense matter in their interior. The damping of density perturbations, described locally by the bulk viscosity, is particularly important since it has been shown to vary greatly between different phases [1–14]. In addition to the damping properties of bulk phases, the boundary between different phases can also be relevant for dissipation. A well-known example is Ekman layer damping due to shear forces at the boundary between a fluid and a solid phase [15]. Here we propose a dissipation mechanism that stems from the fact that pressure oscillations can cause the interface between two phases to move back and forth, as the two phases are periodically converted into each other. If the finite rate of this conversion produces a phase lag between the pressure oscillation and the position of the interface, energy will be dissipated in each cycle. We study the resultant damping for the case of a hybrid star with a sharp interface between the quark core and the hadronic mantle, where the dissipation is due to quark-hadron burning at the interface. However, the mechanism is generic and could be relevant for any star with an internal interface, e.g. between neutron and hyperonic matter or between different phases of (color superconducting) quark matter. Unstable global oscillation modes [16] are of particular interest since they arise spontaneously and grow until stopped by some saturation (nonlinear damping) mechanism. For neutron stars, the most important example is r-modes [17, 18] since they can be unstable in typical millisecond pulsars. Several saturation mechanisms have been proposed so far [19–24]. Although bulk viscosity has a nonlinear “suprathermal” regime [3, 25, 26], it has been found that this becomes relevant only at very high amplitudes, and is probably pre-empted by some other stronger mechanism [22]. In this paper we show that dissipation due to hadron-quark burning could well be the dominant saturation mechanism in hybrid stars. The dissipation is vanishingly small at low amplitude, but becomes very strong once the oscillation reaches a critical amplitude. (For similar behavior in a different context see [24]). This strong dissipation saturates unstable r-modes just above the critical ampli-

tude and therefore leads to a simple analytic prediction for the saturation amplitude, which, however, depends sensitively on the velocity of the combustion front which is not known at this point. We find that the r-mode saturation amplitude can be as low as $\alpha_{\text{sat}} \approx 10^{-5}$ for conditions present in observed pulsars. Inclusion of effects arising from the acceleration of the front could reduce the saturation amplitude further.

II. TOY MODEL FOR THE DISSIPATION DUE TO PHASE TRANSFORMATION

A. Piston picture

As a step towards an analysis of the dissipation due to phase conversion in an inhomogeneous multi-component star, we now construct a simplified version of the interface between different layers in a gravitationally bound system. We will calculate the energy dissipated in this system when it is subjected to periodic compression and rarefaction.

Our toy system involves two incompressible phases, characterized by different densities of a conserved particle species. We assume there is a first-order pressure-induced phase transition, so the phases are separated by a sharp interface (“the phase boundary”) which, in long-term equilibrium, is at the critical pressure p_{crit} , and that there are processes that can convert each phase into the other at some finite rate. We consider a cylinder containing both phases in a homogeneous (Newtonian) gravitational field, with a piston which can be moved parallel to the direction of the field (Fig. 1). The high-density phase is deeper in the gravitational potential than the low-density phase. The field produces a pressure gradient in the cylinder, which can be shifted by moving the piston. This will cause the equilibrium position of the interface to shift, but, crucially, depending on the speed of the conversion process, it may take some time for the interface to move to its new equilibrium position. This causes the response of the system (its volume or density) to fall out of phase with the externally applied force, resulting in dissipation. To calculate the energy dissipated per cycle, we simply calculate the net $p dV$ work done by

the piston in one cycle.

We will assume that the equation of state of the two phases is linear,

$$p(\mu) = \begin{cases} \mu n_L - \varepsilon_L & \text{low density phase} \\ \mu n_H - \varepsilon_H & \text{high density phase} \end{cases}, \quad (1)$$

where μ is the chemical potential for the conserved particle number, and the two incompressible phases have fixed particle number densities n_L and n_H , and fixed energy densities ε_L and ε_H . Later we will use the fact that this is a valid approximation for any equation of state, as long as the pressure oscillations are small enough.

In a Newtonian gravitational field the pressure is a function of x determined by

$$\frac{dp}{dx} = -g\varepsilon, \quad (2)$$

where g is the gravitational acceleration, assumed to be independent of x . Eq. (2) has a simple solution where the pressure varies linearly with x , with a fixed gradient $g\varepsilon$ in each phase (see Fig. 2)

$$p(x) = \begin{cases} p_b - g\varepsilon_H(x - x_b) & x < x_b \\ p_b - g\varepsilon_L(x - x_b) & x \geq x_b \end{cases}, \quad (3)$$

where x_b is the position of the interface between the two phases (“the boundary”) and p_b is the pressure at the boundary. In long-term equilibrium, the boundary settles at its “ideal” position, where p_b is p_{crit} (see below).

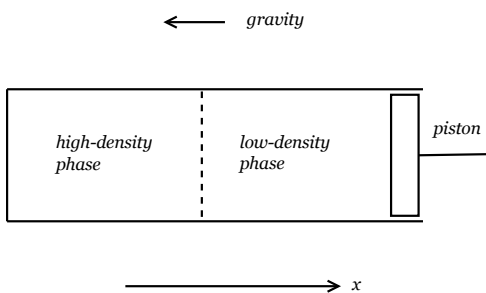


FIG. 1: Toy model: two incompressible phases in a cylinder with piston, in a gravitational field. An oscillation of the external pressure on the piston leads to interconversion of the two phases, and hence movement of the piston.

B. External pressure oscillation

Assume that the external pressure on the piston varies periodically. When the pressure is high, part of the low-density phase is driven to a pressure above p_{crit} and starts

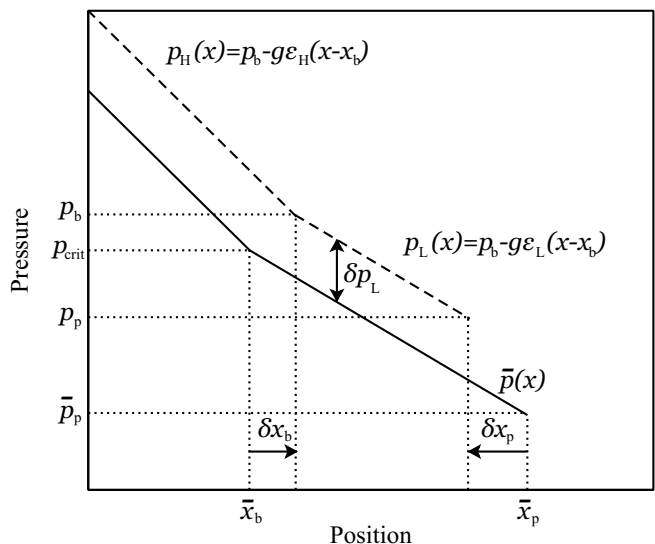


FIG. 2: Pressure gradients in the cylinder of Fig. 1. Solid line $\bar{p}(x)$ is the pressure profile in beta equilibrium. This snapshot captures the system at a moment when the piston has moved in a distance δx_p , the pressure has risen, and the boundary has moved out a distance δx_b as the low density phase in regions with $p > p_{\text{crit}}$ converts to the high-density phase.

to convert into the high density phase, and vice versa during rarefaction. The pressure and the position of the phase boundary therefore vary,

$$p(x, t) = \bar{p}(x) + \delta p(x, t), \quad (4)$$

$$x_b(t) = \bar{x}_b + \delta x_b(t), \quad (5)$$

where \bar{x}_b is the equilibrium position of the boundary and $\bar{p}(x)$ is the pressure profile in beta equilibrium. The position of the boundary at a given moment depends on the previous compression history and the phase conversion rate, and we expect that, because of the finite rate of conversion between the two phases, the oscillation of the boundary can be out of phase with the oscillation of the pressure, and this will lead to dissipation via net $p dV$ work being done in each cycle.

To calculate the dissipation, we need to relate the movement of the boundary to the applied pressure oscillation. We assume that the pressure in the low density phase oscillates harmonically with amplitude Δp_L and frequency ω , so $\delta p_L(t) = \Delta p_L \sin(\omega t)$.

In equilibrium, the piston is at \bar{x}_p with pressure \bar{p}_p . As part of the pressure oscillation the piston moves

$$x_p(t) = \bar{x}_p + \delta x_p(t), \quad (6)$$

and the pressure at the piston is

$$p_p(t) = \bar{p}_p - g\varepsilon_L \delta x_p(t) + \Delta p_L \sin(\omega t) \quad (7)$$

The movement of the piston and the movement of the phase boundary are connected by particle number conservation inside the cylinder. The total particle number

is $N_{\text{tot}} = (x_{\text{b}}(t)n_{\text{H}} + (x_{\text{p}}(t) - x_{\text{b}}(t))n_{\text{Q}})S$ where S is the cross sectional area. Particle number conservation $\delta N_{\text{tot}} = 0$ gives

$$x_{\text{p}}(t) = \bar{x}_{\text{p}} + \left(1 - \frac{n_{\text{H}}}{n_{\text{L}}}\right) \delta x_{\text{b}}(t). \quad (8)$$

We can now express the $p dV$ work done by the piston in one cycle in terms of the movement of the boundary δx_{b} induced by the pressure oscillation. In later sections we will study how the boundary moves, expressing it as a function of the speed of the phase conversion process. First, however, we define a useful concept, the ‘‘ideal boundary’’.

C. Ideal position of the phase boundary

In discussing the motion of the boundary it is convenient to define an ‘‘ideal position’’ of the boundary, x_{ib} . Since we are assuming that an external force imposes a specified time-dependence of the pressure in the low-density phase, it is natural to define the ideal boundary at time t to be the position the boundary would reach if we held p_{L} fixed at its current value and waited for weak interactions to equilibrate. Thus $x_{\text{ib}}(t)$ is the solution of $p_{\text{L}}(x_{\text{ib}}, t) = p_{\text{crit}}$. Unlike the actual boundary, the ideal boundary is determined simply by the instantaneous value of the applied pressure, with no dependence on previous history or conversion rate. The position of the ideal boundary therefore oscillates in phase with the pressure,

$$\delta x_{\text{ib}}(t) = \Delta x_{\text{ib}} \sin(\omega t), \quad \Delta x_{\text{ib}} = \frac{\Delta p_{\text{L}}}{g\varepsilon_{\text{L}}} \quad (9)$$

and its velocity is 90° out of phase

$$v_{\text{ib}}(t) = v_{\text{ib}}^{\text{max}} \cos(\omega t), \quad v_{\text{ib}}^{\text{max}} = \omega \Delta x_{\text{ib}} = \frac{\omega \Delta p_{\text{L}}}{g\varepsilon_{\text{L}}}. \quad (10)$$

For a harmonic pressure oscillation in the low-density phase the ideal boundary moves harmonically. Note however, that because of the discontinuity in energy density on the phase boundary, the pressure oscillation cannot be simultaneously harmonic in both phases. It is also worth noting that using our definition $x_{\text{ib}}(t)$ is not in general the place in the cylinder where the pressure at time t is p_{crit} : these locations only coincide if the real phase boundary occurs where the pressure is above p_{crit} .

D. Energy dissipation in one cycle

The net $p dV$ work done by the piston in one cycle ($0 \leq t < \tau$, $\tau = 2\pi/\omega$) is

$$W = -S \int_0^\tau p_{\text{p}}(t) \frac{dx_{\text{p}}(t)}{dt} dt \quad (11)$$

where p_{p} is the pressure at the location of the piston, which is determined by the applied oscillation of the piston, and x_{p} is the position of the piston, which depends on the movement of the actual boundary Eq. (8).

To obtain $\delta x_{\text{b}}(t)$ we will assume that the conversion process sets an upper limit on how fast the boundary can move, and that the boundary takes a negligible time to accelerate to that velocity. In general, the phase boundary has different maximum velocities when moving inward versus outward, which are determined by microscopic physics, and is independent of the oscillation amplitude. The slower one which we will call v_{b} is crucial to the threshold of energy dissipation.

In effect, the real boundary is always chasing the ideal boundary (which is its long run equilibrium position), while the ideal boundary is a moving target, its sinusoidal movement linearly related to the applied pressure oscillation, see Eqs. (7) and (9).

This leads to two relevant regimes for dissipation.

- (1) $v_{\text{ib}}^{\text{max}} \leq v_{\text{b}}$ no dissipation
 - (2) $v_{\text{ib}}^{\text{max}} > v_{\text{b}}$ finite dissipation
- (12)

Whereas at the onset of regime (2) dissipation arises from a small fraction of the oscillation cycle, at higher amplitude different cases have to be distinguished to compute the dissipation. However, we will see that the dissipation is strong enough to prevent the mode from growing large enough to reach these more complicated cases, so we only discuss the dissipation just above threshold.

Regime (1): no dissipation

In regime (1) the pressure oscillation has such a low amplitude that the ideal boundary does not move far during a cycle, and its maximum velocity is always less than the maximum velocity of the real boundary. The real boundary can therefore remain on top of the ideal boundary at all times, and the system is never forced out of equilibrium. The motion of the boundary and the position of the piston are both in phase with the pressure oscillation, so from Eq. (11) there is no dissipation.

Regime (2): non-zero dissipation

If the maximum speed of the ideal boundary during the pressure cycle ($v_{\text{ib}}^{\text{max}}$) becomes larger than v_{b} , the slower of the real boundary’s two maximum speeds (one for each direction), then the real boundary starts to lag behind the ideal boundary over part of the cycle. This is illustrated in Fig. 3, where the dashed line is the position of the ideal boundary and the solid line is the position of the actual boundary. The real boundary is able to stay on top of the ideal boundary for most of the cycle, but it falls behind at time t_1 , determined by $v_{\text{ib}}(t_1) = v_{\text{b}}$, when the ideal boundary starts moving too fast, and catches up again at time t_2 , determined by $\delta x_{\text{b}}(t_2) = \delta x_{\text{ib}}(t_2)$, when the ideal boundary has slowed down enough. The pressure at the piston and its position are again given by Eq. (7) and Eq. (8). From Eq. (11), the energy dissipa-

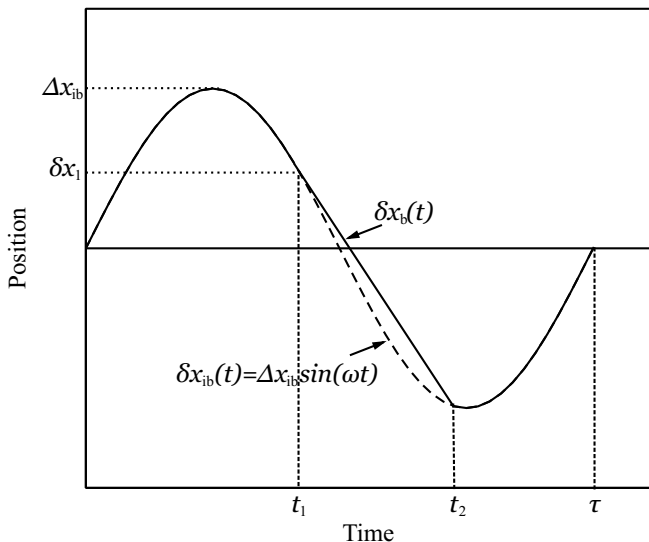


FIG. 3: Movement of the real boundary (solid line) during one pressure cycle, when the pressure oscillation is just large enough so that during part of the cycle the ideal boundary (dashed line) has a speed a little greater than the real boundary's maximum speed.

tion in one cycle is

$$W = S \left(\frac{n_H}{n_L} - 1 \right) \left(\int_0^\tau \bar{p}_p \frac{d\delta x_b(t)}{dt} dt + \int_0^\tau \Delta p_L \sin(\omega t) \frac{d\delta x_b(t)}{dt} dt \right) \quad (13)$$

where the variation in the boundary position is

$$\delta x_b(t) = \begin{cases} \delta x_1 - v_b(t - t_1) & t_1 \leq t < t_2 \\ \delta x_{ib}(t) & \text{otherwise} \end{cases} \quad (14)$$

and δx_1 is shown in Fig. 3. Using Eq. (14), the first line of W vanishes and

$$W = S \left(\frac{n_H}{n_L} - 1 \right) \frac{v_b \tau}{\pi} \Delta p_L \frac{\eta + \cos \beta}{2} \quad (15)$$

where $\eta \equiv v_b/v_{ib}^{\max}$ and β is the solution of

$$\sqrt{1 - \eta^2} = \sin \beta - \eta [\arccos(-\eta) - \beta]. \quad (16)$$

In the limit $v_b \rightarrow v_{ib}^{\max}$, the energy dissipation per cycle is

$$W = \frac{3}{2} S \left(\frac{n_H}{n_L} - 1 \right) \frac{v_b \tau}{\pi} \Delta p_L \left(1 - \frac{v_b}{v_{ib}^{\max}} \right) \quad (17)$$

We see that the dissipation vanishes if the two phases have equal densities, since then the movement of the phase boundary does not change the volume of the system, so there is no associated $p dV$ work. If $v_{ib}^{\max} < v_b$ then we are in the “no dissipation” regime.

To derive the dissipation we assumed that the pressure oscillation in the low density phase is harmonic.

Had we instead assumed that the pressure oscillation in the high density phase is harmonic, then the energy dissipation would be slightly bigger, with a difference $\Delta W/W \simeq \Delta \varepsilon/\varepsilon_L$, where $\Delta \varepsilon$ is the energy density discontinuity at the interface.

III. R-MODE DAMPING AND SATURATION

We can now calculate the damping of a global oscillation mode in a hybrid star resulting from the phase conversion mechanism. A comprehensive analysis of this problem requires the detailed density oscillation of the global mode in a star with multiple components separated by density discontinuities due to first order phase transitions. So far the profiles for global oscillation modes have not been obtained for such a realistic model of a compact star. We will therefore estimate the dissipation from a piecewise model for the mode profile, using the known form for a homogenous star on either side of the phase boundary. We estimate the error due to this simplified procedure below. Although the amplitude of the mode's density and pressure oscillation varies from place to place in the star, the simple piston picture sketched above then applies locally for sufficiently small volume elements containing the interface between the two phases and the entire range over which it moves in response to the oscillation.

Here we study the case of r-modes since they are unstable and require a sufficiently powerful damping mechanism to ensure that they do not spin down the fast rotating compact stars that we observe. The density fluctuation for an $m=2$ r-mode to leading order in the mode amplitude α is [27]

$$\frac{\delta \varepsilon}{\bar{\varepsilon}} = \sqrt{\frac{8}{189}} \alpha A R^2 \Omega^2 \left(\frac{r}{R} \right)^3 \text{Re} [Y_3^2(\theta, \phi) e^{i\omega t}] \quad (18)$$

where $\delta \varepsilon = \varepsilon - \bar{\varepsilon}$, $Y_3^2(\theta, \phi) = \frac{1}{4} \sqrt{\frac{105}{2\pi}} e^{2i\phi} \sin^2 \theta \cos \theta$, and A is the inverse speed of sound squared

$$A \equiv \frac{\partial \varepsilon}{\partial p} \quad (19)$$

evaluated at equilibrium.

The r-mode involves flows that are dominantly angular rather than radial. At any moment there is higher pressure in some regions of solid angle in the star, and lower pressure in other regions. This means that globally the fraction of high or low pressure phase does not change much over time. However, an r-mode will still lead to conversion between the phases, since the low and high pressure regions are kilometers apart, so the gradients of pressure and density in the angular directions are extremely small, and in an oscillation at kHz frequencies there is not enough time for any response other than movement of the boundary in the radial direction. Therefore particle transformation is required in far-separated

areas despite the approximate global conservation of the amount of each of the two forms of matter. The simple cylinder and piston model of Sec. II is a valid approximation for a small volume element that straddles the interface between the two phases. To use the results from Sec. II we simply need to use the appropriate expression for the local gravitational acceleration g . The general relativistic generalization of the Newtonian hydrostatic equation is the Oppenheimer-Volkoff (OV) equation [28]

$$\begin{aligned} \frac{dp}{dr} &= -g_{\text{eff}}(r) \epsilon(r) \\ g_{\text{eff}}(r) &= \frac{M}{r^2} \left(1 + \frac{p}{\epsilon}\right) \left(1 + \frac{4\pi p r^3}{M}\right) \left(1 - \frac{2M}{r}\right)^{-1} \end{aligned} \quad (20)$$

where p , ϵ and M , given by $(dM)/(dr) = 4\pi r^2 \epsilon$, depending on the radial position. The effective gravitational acceleration g_{eff} contains general relativistic corrections to its Newtonian value M/r^2 .

A. Movement of the ideal boundary

We will now calculate the dissipation of the energy of an r-mode in a star with a high density core surrounded by a low density mantle. (In the next section we will look at the case where the phases are quark matter and hadronic matter.) We are interested in situations where phase conversion dissipation becomes important in r-mode oscillations when their amplitude is still fairly low (we will see in Sec. IV D that this may indeed happen), so we will assume $\delta p \ll \bar{p}$ in the region near the boundary. Therefore, we only need the EoS in a narrow pressure range around the critical pressure. The EoS can be expanded to linear order analogous to Eq. (1) so the pressure oscillation is given by

$$\delta p = \frac{\bar{\epsilon}}{A} \frac{\delta \epsilon}{\bar{\epsilon}}. \quad (21)$$

When $\delta \epsilon > 0$, according to Eq. (18)–(21) the r-mode pressure oscillation in the low density phase is

$$\delta p_{\text{L}}(r, \theta, \phi, t) = \bar{\epsilon}_{\text{L}}(r) C(r) \alpha \sin^2 \theta \cos \theta \cos(2\phi + \omega t) \quad (22)$$

where

$$C(r) \equiv \sqrt{\frac{105}{756\pi}} \Omega^2 \frac{r^3}{R} \quad (23)$$

The ideal boundary position R_{ib} (same as x_{ib} in the previous section) is determined by the r-mode pressure oscillation in the low-density phase, and therefore depends on the angular co-ordinates. If we write $R_{\text{ib}} = \bar{R}_{\text{b}} + \delta R_{\text{ib}}$, where \bar{R}_{b} is the equilibrium position of the phase boundary with no pressure oscillation, then from (20) and (22)

$$\delta R_{\text{ib}}(t) = \frac{\delta p_{\text{L}}}{dp/dr(\bar{R}_{\text{b}})} = \frac{\alpha C_{\text{b}}}{g_{\text{b}}} \sin^2 \theta \cos \theta \cos(2\phi + \omega t) \quad (24)$$

where

$$\begin{aligned} g_{\text{b}} &\equiv g_{\text{eff}}(\bar{R}_{\text{b}}) \\ C_{\text{b}} &\equiv C(\bar{R}_{\text{b}}) = \sqrt{\frac{105}{756\pi}} \Omega^2 \frac{\bar{R}_{\text{b}}^3}{R}. \end{aligned} \quad (25)$$

and $g_{\text{eff}}(\bar{R}_{\text{b}})$ is the effective gravitational acceleration at \bar{R}_{b} evaluated in the low-density phase.

The oscillation amplitude of the ideal boundary position, as a function of latitude θ in the star, is

$$|\delta R_{\text{ib}}| = \frac{C_{\text{b}} \alpha}{g_{\text{b}}} |\sin^2 \theta \cos \theta| \quad (26)$$

and the maximum value of the velocity of the ideal boundary $v_{\text{ib}}^{\text{max}}$ is

$$v_{\text{ib}}^{\text{max}} = \frac{C_{\text{b}} \alpha \omega}{g_{\text{b}}} |\sin^2 \theta \cos \theta| \quad (27)$$

B. R-mode energy dissipation

We now calculate $dW(\theta, \phi)$, the energy dissipated during one oscillation cycle in a radially oriented cylinder straddling the phase boundary, with an infinitesimal base area located at a given spherical angle. Integrating this result over solid angle will give the total dissipation of the r-mode. Using Eqs. (13) and (24),

$$dW(\theta, \phi) = dS \left(\frac{n_{\text{H}}}{n_{\text{L}}} - 1 \right) |\delta p_{\text{L}}| \int_0^\tau \cos(2\phi + \omega t) d\delta R_{\text{b}}(t) \quad (28)$$

where $|\delta p_{\text{L}}| = g_{\text{b}} \epsilon_{\text{crit}}^{\text{L}} |\delta R_{\text{ib}}|$, and from Eq. (26)

$$|\delta p_{\text{L}}| = \epsilon_{\text{crit}}^{\text{L}} C_{\text{b}} \alpha |\sin^2 \theta \cos \theta|, \quad (29)$$

and $dS = \bar{R}_{\text{b}}^2 \sin \theta d\theta d\phi$.

At fixed θ , we perform the time integral in Eq. (28). Depending on the amplitude of the motion of the ideal boundary at that angle, which determines the maximum velocity of the ideal boundary during one cycle, the damping will fall into one of the two regimes described in Sec. II D.

(1) $v_{\text{ib}}^{\text{max}} \leq v_{\text{b}}$, which occurs at angles

$$\alpha \omega |\sin^2 \theta \cos \theta| \leq \frac{v_{\text{b}} g_{\text{b}}}{C_{\text{b}}} \quad (30)$$

has no dissipation, $dW(\theta) = 0$

(2) $v_{\text{ib}}^{\text{max}} > v_{\text{b}}$, which occurs at angles

$$\alpha \omega |\sin^2 \theta \cos \theta| > \frac{v_{\text{b}} g_{\text{b}}}{C_{\text{b}}} \quad (31)$$

has finite dissipation

$$dW(\theta) = dS \left(\frac{n_{\text{H}}}{n_{\text{L}}} - 1 \right) \frac{v_{\text{b}} \tau}{\pi} |\delta p_{\text{L}}| \frac{\eta + \cos \beta}{2} \quad (32)$$

where η and β are the same parameter defined in Eq. (15). In the limit $v_b \rightarrow v_{ib}^{\max}$, Eq. (32) becomes

$$dW(\theta) = \frac{3}{2} dS \left(\frac{n_H}{n_L} - 1 \right) \frac{v_b \tau}{\pi} |\delta p_L| \left(1 - \frac{v_b}{v_{ib}^{\max}} \right) \quad (33)$$

As discussed earlier, these estimates are based on an approximate r-mode profile. To estimate the uncertainty due to this simplification we compare two idealized cases, where the pressure oscillation is harmonic in the low density phase, and where it is harmonic in the high-density phase. As discussed below Eq. (16) the difference for an infinitesimal volume element is of order $\Delta W/W \simeq \Delta \varepsilon/\varepsilon_L$ which directly gives an estimate for the uncertainty of the dissipation in the case of global r-modes. Typical density steps at first order transitions in a compact star are less than a factor of two, but due to the simplified model assumptions we make here our results should anyway be viewed as order of magnitude estimates.

C. Critical and saturation amplitude

Fig. 7 shows the factor arising in Eqs. (30) and (31) as a function of the polar angle. Dissipation only occurs in regions where $dW(\theta)/dS > 0$. At very low r-mode amplitude α , the whole star is in regime 1, with no dissipation. At a critical value α_{crit} , parts of the star enter regime (2), and dissipation rises above zero. In Appendix A we perform the angular integral over the whole star, and show that that when the r-mode amplitude rises slightly above α_{crit} , energy dissipation grows so rapidly that the r-mode will be saturated almost immediately. The saturation amplitude is therefore well approximated by α_{crit} ,

$$\alpha_{\text{sat}} \approx \alpha_{\text{crit}} = \frac{3\sqrt{3}}{2} \frac{v_b g_b}{C_b \omega} \quad (34)$$

where v_b is the lower of the boundary's two maximum velocities (one for each direction); g_b is the effective gravitational acceleration at the phase boundary, and C_b (see Eq. (25)) characterizes the amplitude of the r-mode pressure oscillation at the boundary. The oscillation frequency of the r-mode is $\omega = 2\Omega/3$ (Ω is the angular frequency of star rotation) and the numerical prefactor comes from the fact that $2/(3\sqrt{3})$ is the maximum value of the function $\sin^2\theta \cos\theta$ (Eq. (27)). Note that α_{crit} is determined by the properties of the star, such as its rotation frequency and the size of its higher-density core (via C_b and g_b) and by the speed of the conversion process between the two phases (via v_b). In the next section we will estimate v_b for hadron-quark conversion.

IV. HADRON/QUARK CONVERSION IN A HYBRID STAR

The damping mechanism that we have analyzed above is generic, and will operate in any situation where there

are two phases with a sharp interface. However, the amount of damping depends crucially on the speed v_b at which the interface between the two phases can move, via conversion of one phase into the other. To explore the relevance of this mechanism to a realistic case, we will now estimate the boundary velocity for the example of an interface between strange quark matter and nuclear matter in a hybrid star, and from Eq. (34) obtain an estimate of the r-mode saturation amplitude in this scenario.

There is existing literature, developed in the context of the strange matter hypothesis (that strange quark matter is the true ground state at zero pressure) on the outward-moving burning front that accompanies the transformation of a neutron star into a strange star [29, 30]. Hydrodynamical simulations of the burning process have been performed [31, 32] and possible astrophysical observables (gamma-ray bursts, neutrino emissions and gravitational waves, etc) have been discussed [33, 34]. Our situation is related to this work, but we are interested in conversion of quark matter to nuclear matter as well as nuclear matter to quark matter, since both processes occur as our burning front moves inwards and outwards in response to an oscillation in the pressure.

A. Pressure and chemical potential at the interface

In equilibrium, both pressure and baryon chemical potential are continuous across the phase boundary between nuclear and quark matter, and their values at the boundary are the critical values at which the phase transition occurs ($p = p_{\text{crit}}, \mu_B = \mu_B^{\text{crit}}$). When the system is driven out of equilibrium by global pressure oscillations, the phase boundary may temporarily be at a different pressure because the conversion between nuclear and quark matter has a limited rate. The boundary is then out of chemical equilibrium, and the baryon chemical potential is no longer continuous at the boundary because baryon number cannot flow freely through the boundary. On the timescale of chemical equilibration the pressure is still continuous because it equilibrates at the speed of sound which is of order c . The burning front will move as the phase with higher baryon chemical potential converts into the phase with lower baryon chemical potential. The situation is illustrated in Fig. 4. If the pressure at the boundary is above the critical value ($p_b = p_1 > p_{\text{crit}}$), the baryon number chemical potential in quark matter is lower ($\mu_1^Q < \mu_1^N$). Nuclear matter (NM) is then converted into quark matter (QM) and the front moves outwards. If the pressure at the boundary is below the critical value ($p_b = p_2 < p_{\text{crit}}$) the front moves in the opposite direction converting quark matter back into nuclear matter.

As we will see below, when the boundary is out of chemical equilibrium, and moving to reestablish that equilibrium, it has around it a $\text{NM} \rightleftharpoons \text{QM}$ conversion region, where the matter is out of beta equilibrium. The chemical potential μ_K , which couples to the imbalance

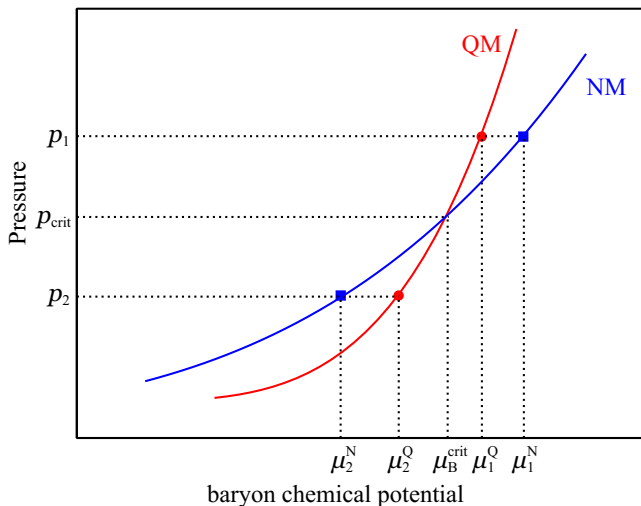


FIG. 4: Schematic plot of the pressure as a function of baryon chemical potential in beta-equilibrated ($\mu_K = 0$) nuclear matter and quark matter. At a given pressure, the phase with lower μ_B is thermodynamically favored.

between strange and down quarks

$$\begin{aligned} \mu_K &\equiv \mu_d - \mu_s, \\ n_K &= \frac{1}{2}(n_d - n_s), \end{aligned} \quad (35)$$

takes a nonzero value in the conversion region; it is zero in beta equilibrated matter. In the following sections we discuss how μ_K and μ_B vary in the conversion region when the front is moving, in order to estimate the speed of the boundary, which determines the energy dissipation.

B. Conversion of nuclear matter into quark matter

To estimate the front speed in the $\text{NM} \rightarrow \text{QM}$ transition when $p_b = p_1 > p_{\text{crit}}$, we use the one-dimensional steady-state approximation used by Olinto [35] to analyze the conversion of neutron matter into strange quark matter. This analysis is conveniently performed in the rest frame of the boundary, where the boundary is at $x = 0$, neutron matter is at $x < 0$ and strange quark matter at $x > 0$. The transformation of neutron matter into strange quark matter requires considerable strangeness production, which can only be accomplished by flavor-changing weak interactions. The slow rate of weak interactions means that at the front nuclear matter is converted in to some form of non-beta-equilibrated quark matter (with $\mu_K \neq 0$). In the conversion region behind the front there are flavor-changing non-leptonic interactions and strangeness diffusion. The weak interactions create strangeness and allow μ_K to return to zero over a distance scale of order $(D_Q \tau_Q)^{1/2}$ where τ_Q is the timescale of the flavor-changing non-leptonic interactions and D_Q is the diffusion constant for flavor. The diffusion of strangeness towards the boundary and downness

away from the boundary allows the strange matter at the boundary to have a strangeness fraction different from that of the nuclear matter which is undergoing deconfinement as the front moves.

The chemical equilibration of quark matter can proceed via the nonleptonic channel $u + s \rightarrow d + u$ and also the leptonic Urca channel $d \rightarrow u + e^- + \bar{\nu}$. Following Ref. [35], we neglect the Urca channel here for simplicity, but we discuss its potential impact in Sec. V.

In general, strangeness gradients could also exist in front of the boundary, as strangeness could diffuse through the boundary, creating (or adding to) hyperons on the nuclear matter side. However, following Ref. [35], we will assume that the front moves fast enough for this effect to be negligible, so $\mu_K = 0$ everywhere ahead of the moving front, i.e. at $x < 0$. The conversion region is then limited to $x > 0$, and can be characterized by $\mu_K(x)$, or equivalently by the K-fraction parameter $a(x)$ which decreases with increasing strangeness fraction

$$a(x) \equiv \frac{n_K(x)}{n_Q} = \frac{n_d - n_s}{2n_Q} \quad (36)$$

where n_Q is the baryon number density in equilibrated strange quark matter.

The spatial variation of a (Fig. 5, right panel) is determined by the steady-state transport equation, written in the rest frame of the boundary,

$$\begin{aligned} D_Q a'' - v_{\text{N} \rightarrow \text{Q}} a' - R(a) &= 0 \\ R(a) &= (\Gamma_{d \rightarrow s} - \Gamma_{s \rightarrow d})/n_Q \end{aligned} \quad (37)$$

where D_Q is the flavor diffusion coefficient, $v_{\text{N} \rightarrow \text{Q}}$ the front speed and $R(a)$ is the net rate of flavor-changing weak interactions. The boundary conditions are

$$\begin{aligned} a(0^-) &\equiv a_1 & a(x \rightarrow +\infty) &\rightarrow 0 \\ a(0^+) &\equiv a_0 & a'(0^+) &= -v_{\text{N} \rightarrow \text{Q}}(a_1 - a_0)/D_Q. \end{aligned} \quad (38)$$

where $a_1 = n_N/n_Q < 1$ and a_0 is the boundary value $a(0^+)$. (Note that this differs from a_0 defined in Ref. [35] which is an intrinsic property of strange quark matter.)

To understand the discontinuity in $a(x)$ across the boundary, let us consider how the chemical potentials vary in the conversion region. The left panel of Fig. 5 shows a schematic plot in the (μ_B, μ_K) plane. The parabolic-looking curve is the quark matter isobar for pressure $p_b = p_1 > p_{\text{crit}}$. The square marked “N” is beta-equilibrated ($\mu_K = 0$) nuclear matter at the same pressure. The spatial variation in the conversion region, shown in the right panel of Fig. 5, can then be mapped on the chemical potential space as follows. At $x < 0$ we have beta-equilibrated nuclear matter (N). At $x = 0$, where $a(x)$ drops from a_1 to a_0 , μ_K jumps to Q^* , which is out-of-equilibrium quark matter with non-zero μ_K , but at the same pressure as the nuclear matter. Then as we traverse the conversion region (increasing x), μ_K decays to zero, finally arriving at equilibrated quark matter

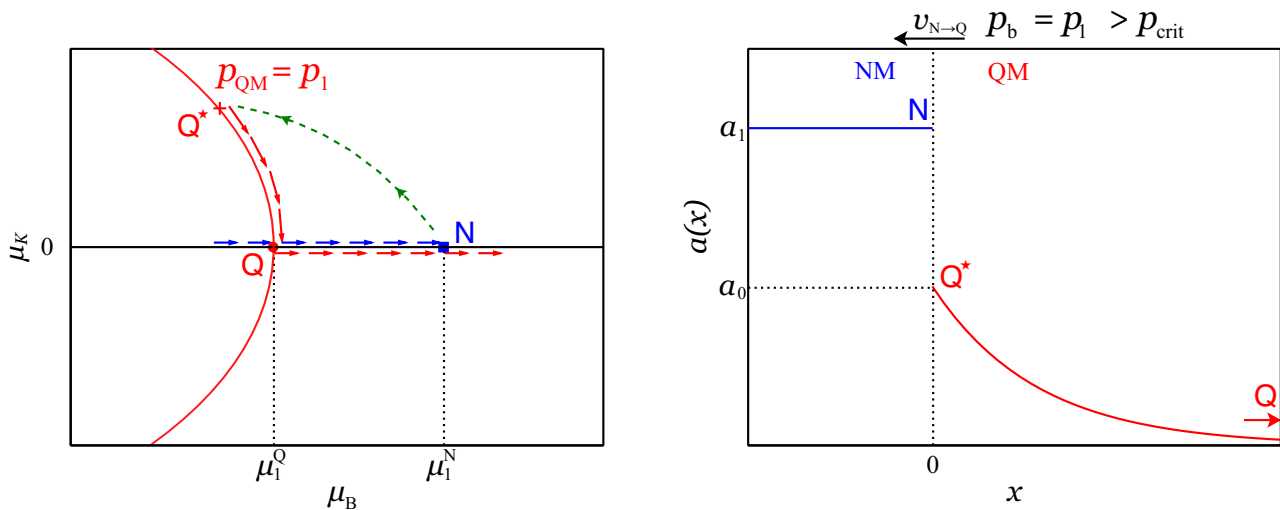


FIG. 5: Conversion of nuclear matter into quark matter. Right panel: spatial variation of quark matter K-fraction parameter a (36) in the conversion region in quark matter. Left panel: corresponding path in the (μ_B, μ_K) plane of chemical potentials.

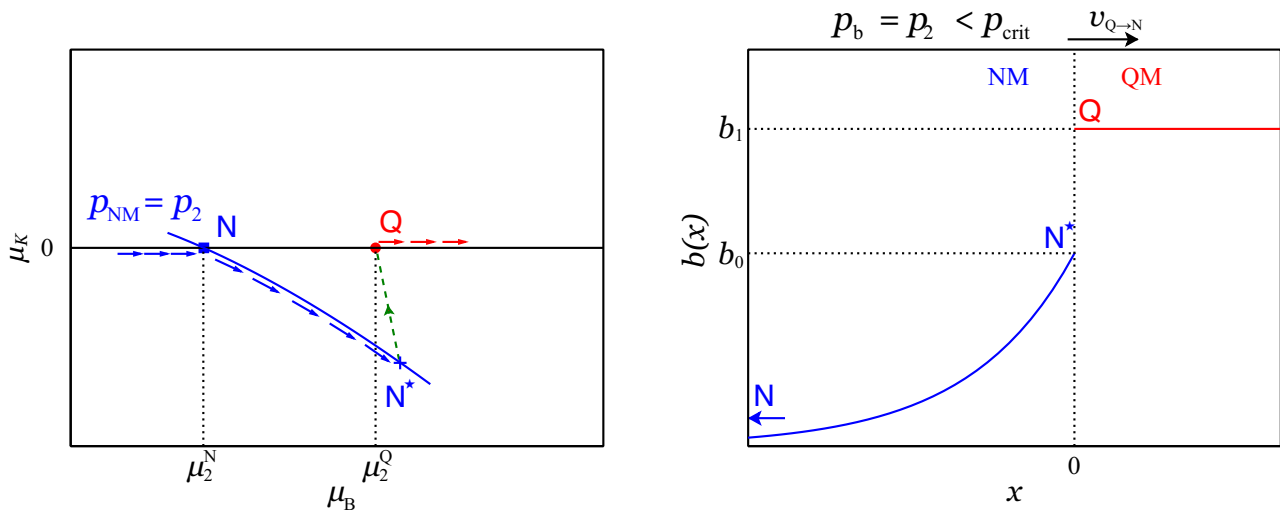


FIG. 6: Conversion of quark matter into nuclear matter. Right panel: spatial variation of nuclear matter K-fraction parameter b (45) in the conversion region in nuclear matter. Left panel: corresponding path in the (μ_B, μ_K) plane of chemical potentials.

(Q). All of these configurations are at the same pressure, based on the assumption that the thickness of the conversion region is negligible when compared to the radius of the star. The arrows along the $\mu_K = 0$ axis show how μ_B varies as one moves larger distances through beta-equilibrated matter on either side of the conversion region, with the pressure rising monotonically. The arrows above the $\mu_K = 0$ axis (blue online) show μ_B increasing as we move inwards through nuclear matter until at N ($\mu_B = \mu_1^N$) we reach the phase boundary. After traversing the phase boundary and conversion region as described above, we are at Q, in beta-equilibrated quark matter at lower μ_B , and as we move into the quark core, μ_B rises again (arrows below $\mu_K = 0$ axis, red online).

Olinto [35] argued that when the phase boundary is

in a steady state of motion there is a “pileup” of nuclear matter in front so that nuclear and quark matter have the same density there, and the boundary has the same velocity relative to nuclear matter and quark matter, i.e. the nuclear matter near the boundary is stationary relative to the quark matter. However, we argue that this is not possible in steady state. When the phase boundary moves, part of the star is transformed from lower density nuclear matter to denser quark matter, and hydrostatic equilibrium requires the star to shrink. This means that in the outer parts of the star the nuclear matter must fall inwards under gravity, so it is moving towards the quark matter. If the inward velocity of the nuclear matter went to zero near the phase boundary, this would require that the “pileup” grows with time, which is not a steady state

situation. Instead, we argue that the baryon number conservation condition is automatically fulfilled because the weight of the outer region of the star pushes nuclear matter in to the front as fast as the front can “consume” it. The density of nuclear matter at the boundary is therefore unchanged by the movement of the boundary, and the nuclear matter velocity takes the value that is determined by baryon number conservation. As we saw in Eqs. (15) and (33), this density step at the phase boundary is crucial for phase-conversion dissipation to occur.

For a fixed value of a_0 , there is only one $v_{N\rightarrow Q}$ which guarantees a solution of Eq. (37) that satisfies the boundary conditions. The analytical approximation for the numeric result of this solution gives the front speed as [35]

$$v_{N\rightarrow Q} \simeq \sqrt{\frac{D_Q}{\tau_Q} \frac{a_0^4}{2a_1(a_1 - a_0)}}. \quad (39)$$

where τ_Q is the timescale of non-leptonic flavor-changing interactions and D_Q is the diffusion constant for flavor. a_0 is expected to lie in the range $0 < a_0 < a_1$. However, the value of a_0 is not fixed by solving the steady-state condition (Eq. (37)) and imposing the boundary conditions (Eq. (38)). Different values of a_0 give different front profiles corresponding to different front velocities. We are therefore forced to treat a_0 as an external parameter.

The value of a_0 can in principle be determined by solving the full time-dependent diffusion equation, tracking the development of the conversion region and the acceleration of the front from some initial configuration. Such a calculation has been performed for analogous conversion fronts in biochemical systems [36–38], and it is found that the final front speed can be independent of the particular initial and boundary conditions over a significant range of diffusion parameters. It would be interesting to study the quark-hadron case in more depth, to see if a similar phenomenon occurs.

To estimate the other factors that determine the front speed we need the strangeness production rate and the diffusion constant. The rate for the non-leptonic strangeness-changing process has been computed in [39] and corrects the previous result given in Ref. [35] by a factor of 24. In the relevant suprathreshold case $T \ll \mu_K \ll \mu_Q$ [52], where μ_Q is the quark chemical potential, the time scale is

$$R(a) \simeq \frac{128}{5\pi^3} G_F^2 \cos^2\theta_c \sin^2\theta_c \mu_Q^5 \left(\frac{a}{3}\right)^3, \quad (40)$$

$$\tau_Q = a^3/R(a). \quad (41)$$

where G_F is the Fermi constant, θ_c the Cabibbo angle, and therefore $\tau_Q \simeq 1.3 \times 10^{-9} \text{ s} (300 \text{ MeV}/\mu_Q)^5$. The diffusion coefficient D_Q depends on the average speed of the quarks and their mean free path, $D_Q \simeq \frac{1}{3} v_Q \lambda_Q$. Estimating quarks moving at nearly the speed of light and $\lambda_Q \simeq 1 \text{ fm} (\mu_Q/T)^2$ [35] we find $D_Q \simeq 10^{-3} \text{ cm}^2 \text{ s}^{-1} (\mu_Q/T)^2$.

Inserting these values the front speed for the NM \rightarrow

QM conversion is

$$v_{N\rightarrow Q} \simeq (220 \text{ km s}^{-1}) \frac{a_0^2}{\sqrt{a_1(a_1 - a_0)}} \times \left(\frac{\mu_Q}{300 \text{ MeV}}\right)^{7/2} \left(\frac{10^8 \text{ K}}{T}\right). \quad (42)$$

For $T = 10^8 \text{ K}$, $\mu_Q = 300 \text{ MeV}$ and $a_1 \lesssim 1$, the front speed ranges from 80 km s^{-1} at $a_0 = 0.5$ to 20 ms^{-1} at $a_0 = 0.01$, and a simple dimensional estimate for the thickness of the conversion region is $l_Q \simeq \sqrt{D_Q \tau_Q} \approx 4 \times 10^{-4} \text{ m}$, which is much smaller than the star radius, as expected.

C. Conversion of quark matter into nuclear matter

The conversion from quark matter to nuclear matter has not been analyzed previously because it does not arise if quark matter is absolutely stable. However, it can analogously be described in terms of conversion and diffusion behind the boundary, now on the hadronic side where strangeness is carried by hyperons. There are various hyperons that could be present in dense hadronic matter and correspondingly multiple weak reactions involving these hyperons. For an illustrative calculation we only consider one such process, $n + n \rightarrow p + \Sigma^-$, which is a reasonable choice because Σ^- hyperons are expected to be among the first to appear when nuclear matter is compressed, see e.g. [40]. For simplicity, we also neglect electrons in the system, which is admittedly not a good approximation, but we are only aiming to provide an illustrative example. In this case

$$\mu_K = 2\mu_n - \mu_p - \mu_\Sigma \quad (43)$$

$$n_K = \frac{1}{6}(2n_n - n_p - n_\Sigma). \quad (44)$$

Moving away from the boundary on the hadronic side, into the conversion region, the K density is n_K^0 at $x = 0$ and as $x \rightarrow -\infty$ it grows asymptotically to the constant value \bar{n}_K for equilibrated nuclear matter. In nuclear matter the natural parameter to use is the deviation of the K fraction from its equilibrium value,

$$b(x) \equiv \frac{3(\bar{n}_K - n_K(x))}{n_N} \quad (45)$$

where n_N is the baryon number density in equilibrated nuclear matter. As before we neglect strangeness conversion in front of the boundary, which is the quark matter region in this case. The steady-state transport equation for $b(x)$ in the rest frame of the boundary is

$$D_N b'' + v_{Q\rightarrow N} b' + Q(b) = 0 \quad (46)$$

$$Q(b) = 3(\Gamma_{n+n\rightarrow p+\Sigma^-} - \Gamma_{p+\Sigma^- \rightarrow n+n})/n_N \quad (47)$$

where D_N is the flavor diffusion coefficient, $v_{Q\rightarrow N}$ is the front speed for the QM \rightarrow NM transition and $Q(b)$ the

strangeness-changing reaction rate divided by the baryon number density in nuclear matter. The boundary conditions are

$$\begin{aligned} b(0^-) &= 3n_K^0/n_N \equiv b_0 & b(x \rightarrow -\infty) &\rightarrow 0 \\ b(0^+) &= 3\bar{n}_K/n_N \equiv b_1 & b'(0^-) &= v_{Q \rightarrow N}(b_1 - b_0)/D_N. \end{aligned} \quad (48)$$

The right panel of Fig. 6 shows how $b(x)$ varies through the phase boundary and transition region. The left panel of Fig. 6 shows schematically the behavior in the (μ_B, μ_K) plane. The short curve through N and N* is the nuclear matter isobar for pressure $p_b = p_2 < p_{\text{crit}}$. The dot marked “Q” is beta-equilibrated quark matter at the same pressure, which exists (see right panel) at $x = 0^+$. The point N* is out-of-equilibrium nuclear matter which is found just behind the boundary at $x = 0^-$. The point N is beta-equilibrated nuclear matter, which is found at the tailing end of the conversion region. All these forms of matter are at the same pressure as long as thickness of the conversion region is much smaller than the radius of the star. The arrows represent how the chemical composition changes as one moves from the hadronic outer part of the star through the conversion region to the quark core. At the boundary $\mu_2^N < \mu_2^Q$ and μ_K in out-of-equilibrium nuclear matter is negative because of the presence of massive hyperons.

Following the same logic as in the previous section, we find the analytic approximation for the front speed

$$v_{Q \rightarrow N} \simeq \sqrt{\frac{D_N}{\tau_N} \frac{b_0^4}{2b_1(b_1 - b_0)}}, \quad (49)$$

where the time scale of the weak interactions is $\tau_N \simeq 27(n_K - \bar{n}_K)^3 / (n_N^3 Q(b))$, where [6]

$$\begin{aligned} n_N Q(b) &\simeq \frac{2}{(2\pi)^5} G_F^2 \cos^2 \theta_c \sin^2 \theta_c \chi m_n^{*2} m_p^* m_\Sigma^* k_F^\Sigma \\ &\times [B_K (n_K - \bar{n}_K)]^3 \end{aligned} \quad (50)$$

where χ is determined by the reduced symmetric and antisymmetric coupling constants with typical value ~ 0.1 and $B_K \equiv \partial \mu_K / \partial n_K$ is evaluated at $\mu_K = 0$. Both k_F^Σ and B_K are functions of n_N , depending on the nuclear matter EoS.

To estimate the diffusion coefficient $D_N \simeq \frac{1}{3} v_N \lambda_N$ we estimate v_N by the Fermi velocity of hyperons ($v_N \simeq v_F^\Sigma = k_F^\Sigma / m_\Sigma^*$), and the mean free path by $\lambda_N \simeq v_F^\Sigma / \nu_{n\Sigma}$, where $\nu_{n\Sigma}$ is the hadron/hyperon collision frequency similar to the hadron/hadron collision frequency ν_{np} (see Eq. (55) of [41]). As a result,

$$D_N \simeq \frac{m_n^2 k_F^{\Sigma 2}}{32 m_n^* m_\Sigma^{*4} T^2 S_{n\Sigma}(k_F^n, k_F^\Sigma)} \quad (51)$$

where $S_{n\Sigma}$ is the effective hadron/hyperon scattering cross section which we for simplicity approximate by the proton/neutron cross section given in Eq. (58) of [41].

Given the nuclear matter EoS, k_F^Σ and $S_{n\Sigma}$ can be expressed in terms of one single parameter n_N . Here we apply the simple free-gas hadron/hyperon model, calculate τ_N and D_N numerically then fit the speed of the front in QM \rightarrow NM transition to a power law dependence on the temperature and baryon number density. The parametrized expression for $v_{Q \rightarrow N}$ takes the form

$$\begin{aligned} v_{Q \rightarrow N} &\simeq (4 \text{ km s}^{-1}) \frac{b_0^2}{\sqrt{b_1(b_1 - b_0)}} \\ &\times \left(\frac{n_N}{n_0} - 2.237 \right)^{0.5} \left(\frac{10^8 \text{ K}}{T} \right), \end{aligned} \quad (52)$$

and it is valid sufficiently ($\simeq 20\%$) above the Σ -hyperon threshold density in nuclear matter $n_N \approx 2.2 n_0$ and should not be valid above $5 n_0$, due to the involved approximations and the limited range of the fitting function $S_{n\Sigma}$ used in the collision frequency [41].

To compare front speeds in both directions one can impose the pressure equilibrium condition $p_{\text{QM}}(\mu_Q) = p_{\text{NM}}(n_N) = p_{\text{crit}}$ to relate the values of μ_Q and n_N in Eq. (42) and Eq. (52). If we apply a free-gas EoS for nuclear matter and the MIT bag model for quark matter, then equilibrium values near the boundary are $\mu_Q \simeq 365 \text{ MeV}$, $n_Q/n_0 \simeq 4$ and $n_N/n_0 \simeq 2.7$, with the bag constant in quark matter $B = (175 \text{ MeV})^4$ which gives the critical pressure $p_{\text{crit}} \simeq 4.2 \times 10^8 \text{ MeV}^4$. For $T = 10^8 \text{ K}$, the speed of the front in two directions are

$$v_{N \rightarrow Q} \simeq (430 \text{ km s}^{-1}) \frac{a_0^2}{\sqrt{a_1(a_1 - a_0)}} \quad (53)$$

$$v_{Q \rightarrow N} \simeq (2.75 \text{ km s}^{-1}) \frac{b_0^2}{\sqrt{b_1(b_1 - b_0)}} \quad (54)$$

where $a_1 = n_N/n_Q \simeq 0.675$ and $b_1 = 3\bar{n}_K/n_N \simeq 1$. Boundary values a_0 (in Eq. (39)) and b_0 (in Eq. (49)) are not known precisely. If we assume $b_0 \simeq a_0$, then for a_0 and b_0 in $[0.01, 0.5]$, we have $v_{N \rightarrow Q}$ ranges from 50 m s^{-1} to 250 km s^{-1} and $v_{Q \rightarrow N}$ from 0.3 m s^{-1} to 1 km s^{-1} , therefore $v_{N \rightarrow Q} \simeq 200 v_{Q \rightarrow N}$.

D. Effect on dissipated energy and saturation amplitude

If the phase boundary has different maximum velocities when moving inward versus outward (for example $v_{Q \rightarrow N} \ll v_{N \rightarrow Q}$ as we estimated in the previous section) where $v_b = \min[v_{Q \rightarrow N}, v_{N \rightarrow Q}]$, then as the r-mode amplitude grows from small values it is the conversion process with slower-moving boundary that determines the threshold of energy dissipation, which corresponds to $v_b = v_{\text{ib}}^{\text{max}}$. According to Eq. (34), the saturation amplitude of the r-mode has a frequency and temperature

dependence given by

$$\alpha_{\text{sat}}(f, T) \approx \hat{\alpha}_{\text{crit}} \left(\frac{f}{1\text{kHz}} \right)^{-3} \left(\frac{T}{10^8\text{K}} \right)^{-1} \quad (55)$$

$$\hat{\alpha}_{\text{crit}} \approx 3.6 \times 10^{-5} \left(\frac{v_b}{\text{m s}^{-1}} \right) (g_b \bar{R}_b) \left(\frac{R}{\bar{R}_b} \right) \left(\frac{\bar{R}_b}{5\text{km}} \right)^{-3} \quad (56)$$

where R is the star radius, \bar{R}_b is the size of the quark matter core and g_b is the effective gravitational acceleration at \bar{R}_b , evaluated in the low-density phase (see Eq. (25) and Eq. (20)). For instance for v_b between 0.3 m s^{-1} and 1 km s^{-1} (estimates based on Eq. (54)) in typical hybrid star model we get $\hat{\alpha}_{\text{crit}}$ in the range 10^{-5} to 0.025.

If the real phase boundary moves in both directions with the same speed $v_{\text{N} \rightarrow \text{Q}} = v_{\text{Q} \rightarrow \text{N}} = v_b$, then both conversion processes contribute to dissipation as long as $v_b < v_{\text{ib}}^{\text{max}}$, and the dissipated energy is twice the previous result $W' = 2W$ (see Eq. (17)). The critical value of α is the same as given by Eq. (34), whereas the saturation amplitude α_{sat} is slightly closer to the critical amplitude α_{crit} , but since the saturation amplitude is anyway virtually indistinguishable from the critical amplitude (see Appendix A) this does not change our results.

These values of saturation amplitudes (Eq. (55)) should be compared to those that follow from other proposed saturation mechanisms. As noted before the suprathreshold enhancement of the bulk viscosity in the core of a neutron or quark star can only saturate r-modes at large amplitudes $\alpha_{\text{sat}} = O(1)$ [22]. Hydrodynamic oscillations give similarly large values for the saturation amplitude [19]. The non-linear coupling of the r-mode to viscously damped daughter modes is a more effective saturation mechanism and could give values in the range $\alpha_{\text{sat}} = O(10^{-6} - 10^{-3})$ [23, 42]. Finally, the recently proposed vortex/fluxtube cutting mechanism [24], which is analogous to the mechanism presented here, does not dissipate any energy at small amplitudes, could give similarly low amplitudes but is present only at sufficiently low temperatures. We conclude that the mechanism proposed here could, within the considerable uncertainties inherent in present analyses be competitive with other saturation mechanisms.

V. CONCLUSION

We have described a dissipation mechanism in a multi-component compact star that stems from the phase-lagged response of the interface between components of different baryon densities to an applied pressure oscillation. The phase lag arises from the finite rate of interconversion between the phases, which limits the speed with which the interface can move. We studied the case where the two phases are separated by a sharp boundary (first order phase transition). The analysis is done in the steady-state approximation, assuming that the interface moves at a fixed speed. Complicated hydrodynamic effects like turbulence are neglected. In particular, we

studied the astrophysically interesting case of the damping of r-mode oscillations [17, 18] in a two-component star, and found that in the steady-state approximation the dissipation vanishes below a critical r-mode amplitude α_{crit} and rises extremely quickly for $\alpha > \alpha_{\text{crit}}$, so this damping provides a saturation mechanism for r-modes, with saturation amplitude $\alpha_{\text{sat}} \approx \alpha_{\text{crit}}$. In this approach the maximum velocity of the phase boundary is an input parameter, since the steady-state equations do not determine it. We studied the explicit example of hadron-quark transformation at the sharp quark-hadron interface in a hybrid star, and found that the critical r-mode amplitude is expected to be in the range 10^{-5} to 0.1 (Eq. (56)), putting it exactly in the range that is relevant for explaining spindown phenomena like the low spin frequency of young pulsars [43, 44].

Our analysis considered only strangeness-changing non-leptonic processes when we discussed the hadron-quark transformation as an example of phase conversion dissipation. However, there are also leptonic processes that equilibrate the non-strange neutron-proton or up-down ratio. For ordinary bulk viscosity in hadronic or quark matter these processes are only relevant at temperatures far above the temperature of a neutron star because their rate is parametrically smaller than the strangeness changing rate discussed here by a factor of $(T/\mu)^2$ [2]. However, leptonic processes might play an important role in phase conversion dissipation because hadronic matter has more electrons and up quarks than quark matter, so, just as for strangeness, there will be a conversion region behind the moving boundary where conversion and diffusion of up-ness is occurring. Taking this into account could change the estimates given here and should be studied in more detail in the future.

As well as the quark-hadron interface in a hybrid star, any first-order phase transition that leads to a sharp interface between two phases with different baryon densities could, via the mechanism discussed here, cause dissipation of global pressure oscillation modes. One possibility would be different phases of quark matter, perhaps with different Cooper pairing patterns, such as the color-flavor locked (CFL) phase, the 2-flavor color superconductor (2SC) or various forms of inhomogeneous and asymmetric pairing [45], which are all generally connected by first order phase transitions. Because cross-flavor pairing induces shifts in the Fermi surfaces of the participating species, different color superconducting phases will often have different flavor fractions, so movement of the interface between them requires weak interactions, as in the case of the quark-hadron interface. The dissipation mechanism discussed here may therefore be expected to operate, albeit somewhat suppressed by the smallness of the baryon number density differences between these phases.

Our discussion was limited to the case of a sharp interface, which is the expected configuration if the surface tension is large enough. If the surface tension is small there will instead be a mixed phase region where

domains of charged hadronic and quark matter coexist [46, 47]. We expect that the phase conversion dissipation mechanism will operate in this case too, as the domains expand and shrink in response to pressure oscillations. However, to estimate this contribution is far more complicated since it requires us to consider the dynamic formation, growth and merging of these structures, taking in to account the costs and gains due to surface tension and electric field energy. Such an analysis is far beyond the scope of this work, but we expect that the dissipation due to such transformations will be roughly comparable to the estimates given here. A similar mechanism should also be relevant for the “nuclear pasta” mixed phases in the inner crust of an ordinary neutron star. In this case in addition to the slow beta equilibration processes there may also be slow strong interaction equilibration processes, whose rate is suppressed by tunneling factors for the transition between geometric domains of different size. This could further enhance the dissipation.

The phase conversion mechanism for damping relies on the transition between two phases being first order. If there is a crossover then dissipation due to particle conversion is described by the standard bulk viscosity. Examples are the appearance of hyperons in the dense interior or the crossover from npe to $npe\mu$ hadronic matter, where the conserved particle density is lepton number instead of baryon number [48]. The conversion is then not restricted to a thin transition region and partial conversion giving rise to bulk viscosity dissipation takes place all over the relevant part of the star. The additional effect, that the size of the region where muons are present changes as well, is negligible, since the muon fraction continuously goes to zero. This is also reflected by the vanishing of the prefactor in the parenthesis of our general expressions Eq. (13).

In this work, we obtained a reasonable first estimate of the size of the damping by treating the movement of the phase boundary in the steady-state approximation [35], assuming that it can accelerate arbitrarily fast, and that it can move at any speed up to its maximum allowed value, which we estimated using the approach of Ref. [35]. In reality the phase boundary will have to accelerate near the turning points of its motion, and if it cannot accelerate fast enough there will be additional dissipation during this part of the cycle, even if the phase boundary is eventually fast enough (regime (1) in Sec. IID) to stay in chemical equilibrium near the equilibrium position. Our analysis showed that even being out of chemical equilibrium for only a small fraction of a cycle causes the system to dissipate a huge amount of energy, so it is possible that including acceleration effects may yield a much lower r-mode saturation amplitude. This is interesting because it has been shown that r-modes in radio pulsars and low mass x-ray binaries have to have very low amplitudes to be consistent with astrophysical observations [49, 50]. Including the acceleration of the phase boundary will require solving the full time dependent evolution of the phase conversion front, and we plan to address it

in future work.

Appendix A: Angular integral and saturation amplitude

When dissipation first starts to appear, the total dissipated energy in the star is according to Eq. (33)

$$W = \int_0^\pi \int_0^{2\pi} \frac{3}{2} \left(\frac{n_H}{n_L} - 1 \right) \frac{v_b \tau}{\pi} |\delta p_L| \left(1 - \frac{v_b}{v_{ib}^{\max}} \right) dS. \quad (\text{A1})$$

The integral over ϕ gives 2π and the integration interval for θ is $\theta \in [\theta_1, \theta_2] \& [\pi - \theta_2, \pi - \theta_1]$ (see Fig. 7), therefore

$$W = 3\pi \left(\frac{n_H}{n_L} - 1 \right) \frac{v_b \alpha}{\omega} \varepsilon_{\text{crit}}^L C_b \bar{R}_b^2 B \quad (\text{A2})$$

where

$$B(\theta_1, \theta_2) = \left[(\sin^4 \theta_2 - \sin^4 \theta_1) - 4 \frac{v_b g_b}{C_b \alpha \omega} (\cos \theta_2 - \cos \theta_1) \right] \quad (\text{A3})$$

If we write the r-mode amplitude in terms of its critical value α_{crit} as

$$\alpha \equiv (1 + \xi) \alpha_{\text{crit}} \quad (\text{A4})$$

then θ_1 and θ_2 are the solutions of

$$|\sin^2 \theta \cos \theta| = \frac{\frac{2}{3\sqrt{3}}}{1 + \xi} \quad (\text{A5})$$

in the interval $[0, \pi]$, with $\frac{2}{3\sqrt{3}} = |\sin^2 \theta \cos \theta|_{\text{max}}$. And Eq. (A3) becomes

$$B(\xi) = \left[(\sin^4 \theta_2 - \sin^4 \theta_1) - \frac{8}{1 + \xi} \frac{3\sqrt{3}}{3} (\cos \theta_2 - \cos \theta_1) \right] \quad (\text{A6})$$

In the $\xi \ll 1$ limit the approximate solutions of Eq. (A5) are

$$\theta_{1,2} = \theta_{\text{max}} \pm \sqrt{\frac{\xi}{3}} \quad (\text{A7})$$

and Eq. (A6) simplifies to

$$B(\xi) = \frac{16}{9} \sqrt{\frac{2}{3}} \xi^{3/2} \quad (\text{A8})$$

The power emitted by the mode as gravitational radiation can be computed as [51]

$$\left(\frac{d\tilde{E}}{dt} \right)_{\text{GR}} = -\frac{2\tilde{E}}{\tau_{\text{GR}}} \quad (\text{A9})$$

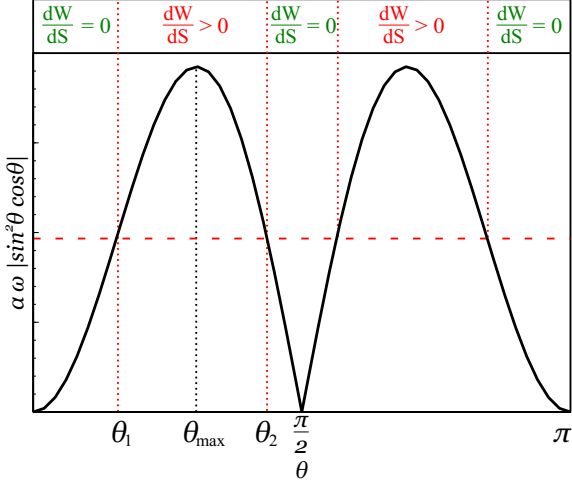


FIG. 7: How non-dissipative ($dW/dS = 0$) and dissipative ($dW/dS > 0$) regimes (Sec. III B) are distributed in a star with an r-mode of amplitude α and frequency ω . We show the polar-angle-dependent amplitude as a function of polar angle θ . The threshold (horizontal dashed line) is given in Eqs. (30) and (31). The solid curve is for an r-mode whose amplitude is large enough to enter the dissipative region at some latitudes in the star.

The expressions for the energy of the mode \tilde{E} and the gravitational radiation time scale in the star are [27, 51]

$$\tilde{E} = \frac{1}{2}\alpha^2\Omega^2 MR^2 \tilde{J} \quad (\text{A10})$$

and

$$\frac{1}{\tau_{\text{GR}}} = -\frac{2^{17}}{3^{85}2^2}\pi G\Omega^6 MR^4 \tilde{J} \quad (\text{A11})$$

The radial integral constant is given by

$$\tilde{J} \equiv \frac{1}{MR^4} \int_0^R \varepsilon(r)r^4 dr \quad (\text{A12})$$

and its typical value for hybrid stars is $\simeq 2 \times 10^{-2}$.

The saturation amplitude $\alpha_{\text{sat}} \equiv (1 + \xi_{\text{sat}})\alpha_{\text{crit}}$ satisfies the equation

$$W \frac{\Omega}{2\pi} = \left(\frac{d\tilde{E}}{dt} \right)_{\text{GR}} \quad (\text{A13})$$

In terms of ξ_{sat} Eq. (A13) reads

$$\frac{B(\xi_{\text{sat}})}{1 + \xi_{\text{sat}}} \left(\frac{n_{\text{H}}}{n_{\text{L}}} - 1 \right) = D \left(\frac{R}{R_{\text{b}}} \right)^8 \frac{g_{\text{b}} GM^2}{\varepsilon_{\text{crit}}^{\text{L}}} \Omega^3 \tilde{J}^2 \quad (\text{A14})$$

with

$$D = \frac{3^{12}\sqrt{3}}{2^{17} \cdot 5^3} \pi^2 \approx 0.554 \quad (\text{A15})$$

From Eq. (A14) we can see that ξ_{sat} is a function of the rotation frequency Ω . For particular hybrid star models one can solve for ξ_{sat} at fixed Ω numerically. Again in the $\xi \ll 1$ limit the analytical expression for ξ_{sat} in Eq. (A14) is:

$$\xi_{\text{sat}}^{3/2} = \left(\frac{n_{\text{H}}}{n_{\text{L}}} - 1 \right)^{-1} \frac{3^{15} \cdot \pi^2}{2^{21} \sqrt{2} \cdot 5^3} \left(\frac{R}{R_{\text{b}}} \right)^8 \frac{g_{\text{b}} GM^2}{\varepsilon_{\text{crit}}^{\text{L}}} \Omega^3 \tilde{J}^2 \quad (\text{A16})$$

which can be written in terms of astrophysical quantities

$$\xi_{\text{sat}} \approx 0.06 \left[\tilde{J}^2 \left(\frac{R}{R_{\text{b}}} \right)^8 \left(\frac{R_{\text{s}}}{R} \right)^{7/2} \left(\frac{\Omega}{\Omega_{\text{K}}} \right)^3 \left(\frac{n_{\text{H}}}{n_{\text{L}}} - 1 \right)^{-1} \frac{g_{\text{b}} \tilde{\varepsilon}}{\tilde{g} \varepsilon_{\text{crit}}^{\text{L}}} \right]^{2/3} \quad (\text{A17})$$

with the Schwarzschild radius $R_{\text{s}} = 2GM$, the Kepler frequency $\Omega_{\text{K}} = \frac{4}{9}\sqrt{2\pi G\tilde{\varepsilon}}$, average gravitational acceleration $\tilde{g} = GM/R^2$ and average energy density $\tilde{\varepsilon} = M/(\frac{4}{3}\pi R^3)$. For most hybrid star models with a quark core bigger than 20% of the star, the value of ξ_{sat} is of the order $10^{-3} \sim 10^{-4}$, which justifies $\alpha_{\text{sat}} \approx \alpha_{\text{crit}}$ in this mechanism.

Acknowledgments

We thank Chuck Horowitz for useful discussions. This research was supported in part by the Office of Nuclear Physics of the U.S. Department of Energy under contract #DE-FG02-05ER41375 and by the DOE Topical Collaboration ‘‘Neutrinos and Nucleosynthesis in Hot and Dense Matter’’, contract #DE-SC0004955.

- [1] R. F. Sawyer, *Bulk viscosity of hot neutron-star matter and the maximum rotation rates of neutron stars*, Phys. Rev. **D39** (1989) 3804–3806.
- [2] P. Haensel and R. Schaeffer, *Bulk viscosity of hot-neutron-star matter from direct URCA processes*, Phys. Rev. **D45** (1992) 4708–4712.
- [3] J. Madsen, *Bulk viscosity of strange dark matter, damping of quark star vibration, and the maximum rotation rate of*

- pulsars*, Phys. Rev. **D46** (1992) 3290–3295.
- [4] P. Haensel, K. P. Levenfish, and D. G. Yakovlev, *Bulk viscosity in superfluid neutron star cores. I. Direct Urca processes in npeμ matter*, Astron. Astrophys. **357** (2000) 1157–1169, [astro-ph/0004183].
- [5] P. Haensel, K. P. Levenfish, and D. G. Yakovlev, *Bulk viscosity in superfluid neutron star cores. II. Modified Urca processes in npeμ matter*, Astron. Astrophys. **327**

- (2001) 130–137, [[astro-ph/0103290](#)].
- [6] P. Haensel, K. P. Levenfish, and D. G. Yakovlev, *Bulk viscosity in superfluid neutron star cores. III. Effects of Σ^- hyperons*, *Astron. Astrophys.* **381** (2002) 1080–1089, [[astro-ph/0110575](#)].
- [7] P. B. Jones, *Bulk viscosity of neutron-star matter*, *Phys. Rev.* **D64** (2001) 084003.
- [8] M. G. Alford and A. Schmitt, *Bulk viscosity in 2SC quark matter*, *J. Phys.* **G34** (2007) 67–102, [[nucl-th/0608019](#)].
- [9] C. Manuel and F. J. Llanes-Estrada, *Bulk viscosity in a cold CFL superfluid*, *JCAP* **0708** (2007) 001, [[arXiv:0705.3909](#)].
- [10] M. G. Alford, M. Braby, S. Reddy, and T. Schafer, *Bulk viscosity due to kaons in color-flavor-locked quark matter*, *Phys. Rev.* **C75** (2007) 055209, [[nucl-th/0701067](#)].
- [11] M. Mannarelli and C. Manuel, *Bulk viscosities of a cold relativistic superfluid: color-flavor locked quark matter*, *Phys. Rev.* **D81** (2010) 043002, [[arXiv:0909.4486](#)].
- [12] X. Wang and I. A. Shovkovy, *Bulk viscosity of spin-one color superconducting strange quark matter*, *Phys. Rev.* **D82** (2010) 085007, [[arXiv:1006.1293](#)].
- [13] K. Schwenzer, *How long-range interactions tune the damping in compact stars*, [arXiv:1212.5242](#).
- [14] C. Manuel, J. Tarrus, and L. Tolos, *Bulk viscosity coefficients due to phonons in superfluid neutron stars*, *JCAP* **1307** (2013) 003, [[arXiv:1302.5447](#)].
- [15] L. Lindblom, B. J. Owen, and G. Ushomirsky, *Effect of a neutron star crust on the r mode instability*, *Phys. Rev.* **D62** (2000) 084030, [[astro-ph/0006242](#)].
- [16] J. L. Friedman and B. F. Schutz, *Secular instability of rotating Newtonian stars*, *Astrophys. J.* **222** (1978) 281.
- [17] N. Andersson, *A new class of unstable modes of rotating relativistic stars*, *Astrophys. J.* **502** (1998) 708–713, [[gr-qc/9706075](#)].
- [18] N. Andersson and K. D. Kokkotas, *The R -mode instability in rotating neutron stars*, *Int. J. Mod. Phys.* **D10** (2001) 381–442, [[gr-qc/0010102](#)].
- [19] L. Lindblom, J. E. Tohline, and M. Vallisneri, *Non-Linear Evolution of the r -Modes in Neutron Stars*, *Phys. Rev. Lett.* **86** (2001) 1152–1155, [[astro-ph/0010653](#)].
- [20] P. Arras *et al.*, *Saturation of the r -mode instability*, *Astrophys. J.* **591** (2003) 1129–1151, [[astro-ph/0202345](#)].
- [21] R. Bondarescu, S. A. Teukolsky, and I. Wasserman, *Spin Evolution of Accreting Neutron Stars: Nonlinear Development of the R -mode Instability*, *Phys. Rev.* **D76** (2007) 064019, [[arXiv:0704.0799](#)].
- [22] M. G. Alford, S. Mahmoodifar, and K. Schwenzer, *Viscous damping of r -modes: Large amplitude saturation*, *Phys. Rev.* **D85** (2012) 044051, [[arXiv:1103.3521](#)].
- [23] R. Bondarescu and I. Wasserman, *Nonlinear Development of the R -Mode Instability and the Maximum Rotation Rate of Neutron Stars*, *Astrophys. J.* **778** (2013) 9, [[arXiv:1305.2335](#)].
- [24] B. Haskell, K. Glampedakis, and N. Andersson, *A new mechanism for saturating unstable r -modes in neutron stars*, [arXiv:1307.0985](#).
- [25] M. G. Alford, S. Mahmoodifar, and K. Schwenzer, *Large amplitude behavior of the bulk viscosity of dense matter*, *J. Phys.* **G37** (2010) 125202, [[arXiv:1005.3769](#)].
- [26] M. G. Alford, S. Reddy, and K. Schwenzer, *Bridging the Gap by Squeezing Superfluid Matter*, *Phys. Rev. Lett.* **108** (2012) 111102, [[arXiv:1110.6213](#)].
- [27] M. Alford, S. Mahmoodifar, and K. Schwenzer, *Viscous damping of r -modes: Small amplitude instability*, *Phys. Rev.* **D85** (2012) 024007, [[arXiv:1012.4883](#)].
- [28] J. Oppenheimer and G. Volkoff, *On Massive neutron cores*, *Phys. Rev.* **55** (1939) 374–381.
- [29] I. Tokareva and A. Nusser, *On the possibility of combustion of neutrons into strange quark matter*, *Phys. Lett.* **B639** (2006) 232–236, [[astro-ph/0502344](#)].
- [30] R. Mallick, A. Bhattacharyya, S. K. Ghosh, and S. Raha, *Conversion of nuclear to 2-flavour quark matter in rotating compact stars: A general relativistic perspective*, [arXiv:0806.1800](#).
- [31] M. Herzog and F. K. Ropke, *Three-dimensional hydrodynamic simulations of the combustion of a neutron star into a quark star*, *Phys. Rev.* **D84** (2011) 083002, [[arXiv:1109.0539](#)].
- [32] G. Pagliara, M. Herzog, and F. Ropke, *Combustion of a neutron star into a strange quark star: The neutrino signal*, *Phys. Rev.* **D87** (2013) 103007, [[arXiv:1304.6884](#)].
- [33] R. Ouyed, D. Leahy, and P. Jaikumar, *Predictions for signatures of the quark-nova in superluminous supernovae*, [arXiv:0911.5424](#).
- [34] T. Chan, K. Cheng, T. Harko, H. Lau, L. Lin, *et al.*, *Could the compact remnant of SN 1987A be a quark star?*, *Astrophys. J.* **695** (2009) 732–746, [[arXiv:0902.0653](#)].
- [35] A. V. Olinto, *On the Conversion of Neutron Stars Into Strange Stars*, *Phys. Lett.* **B192** (1987) 71.
- [36] D. Quinney, *On computing travelling wave solutions in a model for the belousov zhabotinskii reaction*, *IMA Journal of Applied Mathematics* **23** (1979), no. 2 193–201.
- [37] V. Manoranjan and A. Mitchell, *A numerical study of the belousov-zhabotinskii reaction using galerkin finite element methods*, *Journal of Mathematical Biology* **16** (1983), no. 3 251–260.
- [38] J. Murray, *On travelling wave solutions in a model for the belousov-zhabotinskii reaction*, *Journal of Theoretical Biology* **56** (1976), no. 2 329–353.
- [39] J. Madsen, *Rate of the weak reaction $s + u \rightarrow u + d$ in quark matter*, *Phys. Rev.* **D47** (1993) 325–330.
- [40] J. Schaffner and I. N. Mishustin, *Hyperon rich matter in neutron stars*, *Phys. Rev.* **C53** (1996) 1416–1429, [[nucl-th/9506011](#)].
- [41] P. S. Shternin and D. G. Yakovlev, *Shear viscosity in neutron star cores*, *Phys. Rev.* **D78** (2008) 063006, [[arXiv:0808.2018](#)].
- [42] J. Brink, S. A. Teukolsky, and I. Wasserman, *Nonlinear couplings of R -modes: Energy transfer and saturation amplitudes at realistic timescales*, *Phys. Rev.* **D70** (2004) 121501, [[gr-qc/0406085](#)].
- [43] N. Andersson, K. D. Kokkotas, and B. F. Schutz, *Gravitational radiation limit on the spin of young neutron stars*, *Astrophys. J.* **510** (1999) 846, [[astro-ph/9805225](#)].
- [44] M. G. Alford and K. Schwenzer, *Gravitational wave emission and spindown of young pulsars*, [arXiv:1210.6091](#).
- [45] M. G. Alford, A. Schmitt, K. Rajagopal, and T. Schafer, *Color superconductivity in dense quark matter*, *Rev. Mod. Phys.* **80** (2008) 1455–1515, [[arXiv:0709.4635](#)].
- [46] D. G. Ravenhall, C. J. Pethick, and J. R. Wilson, *Structure of matter below nuclear saturation density*, *Phys. Rev. Lett.* **50** (1983) 2066–2069.
- [47] N. K. Glendenning, *First order phase transitions with more than one conserved charge: Consequences for neutron stars*, *Phys. Rev.* **D46** (1992) 1274–1287.

- [48] M. G. Alford and G. Good, *Leptonic contribution to the bulk viscosity of nuclear matter*, [arXiv:1003.1093](#).
- [49] S. Mahmoodifar and T. Strohmayer, *Upper bounds on r -mode amplitudes from observations of LMXB neutron stars*, [arXiv:1302.1204](#).
- [50] M. G. Alford and K. Schwenzer, *What flashes of pulsars can teach us about their interior*, [arXiv:1310.3524](#).
- [51] L. Lindblom, B. J. Owen, and S. M. Morsink, *Gravitational radiation instability in hot young neutron stars*, *Phys. Rev. Lett.* **80** (1998) 4843–4846, [[gr-qc/9803053](#)].
- [52] In the conversion region close to the boundary the quark matter is far from beta equilibrium, so the approximation $\mu_K \ll \mu_Q$ is not always valid, but we have checked that using the full general result makes no significant difference.